doi:10.1093/brain/awu015 Brain 2014: 137; 998–1008 | 998

BRAIN
A JOURNAL OF NEUROLOGY

$Na_V1.4$ mutations cause hypokalaemic periodic paralysis by disrupting IIIS4 movement during recovery

James R. Groome,[1] Frank Lehmann-Horn,[2,3] Chunxiang Fan,[2] Markus Wolf,[2] Vern Winston,[1] Luciano Merlini[4] and Karin Jurkat-Rott[2,3]

1 Department of Biological Sciences, Idaho State University, Pocatello, ID USA 83209, USA
2 Division of Neurophysiology, Ulm University, Ulm, Germany
3 Rare Disease Centre (ZSE) Ulm and Neuromuscular Disease Centre (NMZ) Ulm, University Hospital Ulm, Ulm, Germany
4 Laboratory of Musculoskeletal Cell Biology, Instituto Ortopedico Rizzoli, Bologna, Italy

Correspondence to: James R. Groome,
Department of Biological Sciences,
Gale Life Sciences Bldg,
650 Memorial Drive,
Pocatello, ID USA
E-mail: groojame@isu.edu

Correspondence may also be addressed to: Karin Jurkat-Rott, Division of Neurophysiology, Ulm University, Albert-Einstein-Allee 11 89081 Ulm, Germany, E-mail: karin.jurkat-rott@uni-ulm.de

Hypokalaemic periodic paralysis is typically associated with mutations of voltage sensor residues in calcium or sodium channels of skeletal muscle. To date, causative sodium channel mutations have been studied only for the two outermost arginine residues in S4 voltage sensor segments of domains I to III. These mutations produce depolarization of skeletal muscle fibres in response to reduced extracellular potassium, owing to an inward cation-selective gating pore current activated by hyperpolarization. Here, we describe mutations of the third arginine, R3, in the domain III voltage sensor i.e. an R1135H mutation which was found in two patients in separate families and a novel R1135C mutation identified in a third patient in another family. Muscle fibres from a patient harbouring the R1135H mutation showed increased depolarization tendency at normal and reduced extracellular potassium compatible with the diagnosis. Additionally, amplitude and rise time of action potentials were reduced compared with controls, even for holding potentials at which all $Na_V1.4$ are fully recovered from inactivation. These findings may be because of an outward omega current activated at positive potentials. Expression of R1135H/C in mammalian cells indicates further gating defects that include significantly enhanced entry into inactivation and prolonged recovery that may additionally contribute to action potential inhibition at the physiological resting potential. After S4 immobilization in the outward position, mutant channels produce an inward omega current that most likely depolarizes the resting potential and produces the hypokalaemia-induced weakness. Gating current recordings reveal that mutations at R3 inhibit S4 deactivation before recovery, and molecular dynamics simulations suggest that this defect is caused by disrupted interactions of domain III S2 countercharges with S4 arginines R2 to R4 during repolarization of the membrane. This work reveals a novel mechanism of disrupted S4 translocation for hypokalaemic periodic paralysis mutations at arginine residues located below the gating pore constriction of the voltage sensor module.

Keywords: hypokalaemic periodic paralysis; molecular dynamics; omega pore current; sodium channel; voltage sensor
Abbreviations: NMDG = *N*-methyl-D-glucamine; S4 = segment four

Received August 18, 2013. Revised December 12, 2013. Accepted December 15, 2013. Advance Access publication February 18, 2014

Introduction

Hypokalaemic periodic paralysis is an autosomal dominant skeletal muscle disorder named for recurrent episodes of flaccid limb weakness with reduced ictal serum potassium. Triggering factors for these episodes include carbohydrate-rich meals, rest after exercise, early morning hours, and emotional stress (reviewed by Fontaine, 2008; Cavel-Greant *et al*., 2012). Nearly all causative mutations in hypokalaemic periodic paralysis are associated with the $Ca_V1.1$ calcium channel encoded by *CACNA1S* or the $Na_V1.4$ sodium channel encoded by *SCN4A* (reviewed by Matthews *et al*., 2009). For either of these channels, mutations are located at one of two arginines (R1 or R2) nearest the extracellular end of voltage-sensitive S4 segments, whose movement in response to membrane depolarization is linked to opening of the central conducting pore. Functional expression of channels with R1 or R2 mutations reveals an aberrant leak current through the S4 gating pore (Sokolov *et al*., 2007, 2010; Struyk and Cannon, 2007; Struyk *et al*., 2008; Jurkat-Rott *et al*., 2009; Francis *et al*., 2011). This so-called 'omega' current allows cation influx at the resting state of the sodium channel to depolarize the muscle membrane. Additional depolarization, with reduced conductance of the inwardly rectifying potassium channels by hypokalaemia, impairs the generation of action potentials and leads to muscle weakness (Cannon, 2010; Catterall, 2010; Tricarico and Camerino, 2011; George *et al*., 2012; Jurkat-Rott *et al*., 2012).

Recently, a sporadic case of hypokalaemic periodic paralysis with $Na_V1.4$ mutation R1135H in the domain III voltage sensor was described (Sung *et al*., 2012). Until now, functional expression has not been published for this mutation. However, based on its location (R3) and hypothesized function of the affected S4 segment, the mutant residue should traverse the gating pore of the membrane where the omega current is thought to originate, but only at depolarized potentials in activated or inactivated states of the channel (Sokolov *et al*., 2005). Several R3:DIIS4 mutations in normokalemic periodic paralysis cause an outward omega current at depolarized voltages, which is sustained with inactivation of the channel (Sokolov *et al*., 2008). In this work, we describe R3:DIIIS4 $Na_V1.4$ sodium channel mutations found in hypokalaemic periodic paralysis that promote inward and outward omega currents under different conditions. The clinical presentations for two families with R1135H, and one with a novel R1135C mutation, are compared to the biophysical defects caused by these mutations as observed with electrophysiological recordings from patient muscle fibres or in heterologous expression, and as simulated with molecular dynamics trajectories.

Materials and methods

Families

Whole EDTA blood was taken from patients for *CACNA1S* and *SCN4A* analyses. Complete gene sequencing was performed using PCR amplification and Sanger sequencing as described previously (Jurkat-Rott *et al*., 1994, 2000). Patient studies were approved by the institutional review board in Ulm and conducted according to the Declaration of Helsinki. Informed consent was obtained from patients, and from volunteers with no evidence or history of muscle disease.

Magnetic resonance imaging

^{1}H- and ^{23}Na-MRI of the lower legs of a patient from the HypoPP317 (R1135H) family were performed as described previously (Jurkat-Rott *et al*., 2009).

In vitro studies on native muscle fibres

Muscle specimens were removed from the quadriceps muscles of the index patient of Family HypoPP4 (R1135H) and three adult individuals with no neuromuscular disease under regional anaesthesia. Muscle specimens were ~28 mm in length and 5 mm in diameter. They were further prepared into small bundles and allowed to reseal over 2 h in a solution also used for resting membrane and action potential measurements. This contained (in mM): NaCl 108, KCl 4, $CaCl_2$ 1.5, $MgSO_4$ 0.7, $NaHCO_3$ 26.2, NaH_2PO_4 1.7, Na-gluconate 9.6, glucose 5.5, sucrose 7.6, 290 mOsmol/l, maintained at 37°C, with pH adjusted to 7.4 by bubbling with 95% O_2 and 5% CO_2. In some experiments, extracellular K^+ was decreased to 1 mM.

Membrane potentials were measured by use of a voltage amplifier (Turbo TEC-05, NPI Electronic Instruments) and glass microelectrodes filled with 3 M KCl and input resistances of 5–10 MΩ. Histograms of the potentials were smoothed by density estimation (WARPing). The potentials exhibited a two or three-peak distribution of polarized and depolarized fibres and were displayed as probability density. Parameters were obtained from a Gaussian fit for each peak according to $f(x) = y_0 + (A / w*\mathrm{sqrt}(\pi / 2)) \times \exp(-2 \times ((x - x_n) / w) \wedge 2)$ where y_0 is the minimum asymptote, A is density, and x_n is midpoint voltage.

Action potential recordings were performed with a second microelectrode. This electrode delivered a constant current to hold various resting potentials for at least 1 min to ensure recovery of voltage-gated sodium channels. Then, action potentials were elicited by short depolarizing pulses. The maximum rate of rise was determined at the potential for which the slope of the upstroke of the action potential was maximal. These values were taken as index for the available sodium conductance (Cohen *et al*., 1984) and used to determine slow inactivation parameters by Boltzmann fits. Data are presented as mean ± standard deviation (SD). Statistical significance was assessed by Student's *t*-tests for normally distributed data with a criterion of $P < 0.05$.

Whole cell recording experiments

Site-directed mutagenesis was performed using an overlapping PCR-based technique. Subsequently, the mutants were reassembled in the pRC/CMV plasmid (Invitrogen) for transfection by calcium phosphate precipitation in tsA201, a mammalian cell line. Standard whole cell recording methods were used, as previously described (Kuzmenkin *et al*., 2002). Capacity transients were eliminated by a −p/4 protocol. Series resistance errors were <3 mV and corrections were made for liquid junction potentials. Data were filtered at 3 kHz, and acquired using pCLAMP 10 (Axon Instruments). Patch electrodes contained (in mM): CsF 105, NaCl 35, EGTA 10, Cs-HEPES 10. The bath contained NaCl 150, KCl 2, $CaCl_2$ 1.5, $MgCl_2$ 1, Cs-HEPES 10. Solutions were adjusted to pH 7.4 using CsOH, and experiments were performed at room temperature (20 to 22°C).

Whole cell data for activation, inactivation, and recovery were analysed by a combination of pCLAMP and ORIGIN (MicroCal). Data are

presented as means ± SEM. Statistical significance was assessed by Student's *t*-tests for normally distributed data with a criterion of $P < 0.05$.

Cut-open oocyte experiments

The rat isoform of *SCN4A* in pGEMHE was generously provided by Dr Steven Cannon (University of Southwest Texas Medical Centre, USA). Constructs rR1128H and rR1128C were made using Quik Change XL II site-directed mutagenesis kits (Agilent Technologies) and confirmed by sequence analysis of the coding region. Beta subunit *SCN1B* was housed in pgH19. Plasmids were linearized with NheI (*SCN4A*) or HindIII (*SCN1B*), and messenger RNA was generated using T7 or T3 RNA polymerase (mMESSAGE mMACHINE kits, Ambion). Transcripts were co-injected at a mass ratio of $1\alpha : 3\beta_1$ into oocytes from adult *Xenopus laevis* frogs. Surgical procedures for extraction of oocytes were performed according to IACUC guidelines of the Animal Use and Care Committee at ISU. Oocytes were cultured in medium containing in mM: NaCl 96, KCl 2, $CaCl_2$ 1.8, $MgCl_2$ 1, HEPES 5 and Na pyruvate 2.5, with 100 mg/l gentamicin sulphate and 4% horse serum (Hyclone Laboratories, Fisher Thermo Scientific) at pH 7.4, for 2 to 6 days before recording. All salts and antibiotics were obtained from Sigma Chemical Co.

To record gating and leak currents, we used a CA1B amplifier (Dagan Corporation) with PULSE 8.67 software (HEKA). Oocytes were placed between top and guard chambers. The external solution contained in mM: NMDG (*N*-methyl-D-glucamine) 115, $Ca(OH)_2$ 1.5, BaOH 2.5 and HEPES 10, pH 7.4 adjusted with methanesulphonic acid (Sigma). For external ionic substitution, NMDG was replaced by the hydroxide of Na^+, Li^+ or K^+ 115, or partially by guanidine sulphate 60. The internal solution contained in mM: NMDG 115, EGTA 10 and HEPES 10, pH 7.4, with ionic substitutions the same as above. Before recording, the oocyte was permeabilized with 0.1 to 0.5% saponin to control the electrical and ionic interior of the oocyte. Experiments were started 40 to 50 min later, and ionic currents were blocked with 2 μM tetrodotoxin.

Raw leak currents were recorded with R3 of IIIS4 below or above the gating pore constriction site. To separate background leak from omega currents, the mean current amplitude between 60 to 95 ms of the test potential was taken, and the linear component of the leak current was subtracted from the original I/V relation. For each experiment, leak current amplitudes were normalized against anodic gating charge displaced in response to a 20 ms step depolarization to +40 mV with leak subtraction using −p/8.

In a separate set of experiments the anodic gating charge associated with activation (Ig_{ON}) leading to fast inactivation, and cathodic gating charge associated with subsequent deactivation (Ig_{OFF}) were measured. The integrals of the gating currents Ig_{ON} and Ig_{OFF} were determined and expressed as Ig_{OFF} / Ig_{ON}, as a measure of the return of the available gating charge during S4 translocation preceding recovery. The extent of gating charge return during hyperpolarization was quantified as mean Ig_{OFF} / Ig_{ON} as a function of command voltage.

Molecular dynamics simulations

A homology model of the $rNa_V1.4$ domain III voltage sensor module (S1-S4) was constructed using the A chain of the bacterial sodium channel Na_VAb as template (3RVY.pdb, Payandeh *et al*., 2011), in MODELLER, as described in Groome and Winston (2013). The $rNa_V1.4$ voltage sensor module was embedded in a POPC (1-palmitoyl 2-oleoyl-sn-glycero-3-phosphocholine) lipid bilayer bounded by aqueous layers of 200 mM NaCl using VMD (visual molecular dynamics), and NAMD (not another molecular dynamics) was used for molecular dynamics simulations. Initially, all components of the model except for lipids were constrained for 0.5 ns. The system was then minimized for another 0.5 ns, followed by an equilibration step with protein constrained before 10 ns of free equilibration at a voltage bias of −1200 mV, similar to conditions described in Delemotte *et al*. (2011), Gosselin-Badaroudine *et al*. (2012) and Khalili-Araghi *et al*. (2012). Selected frames were saved as .pdb files. Interatomic distances between DIIIS2 negative countercharges D1066 or E1076 and DIIIS4 arginine residues R2, R3 or R4 were measured with Jmol (Supplementary Table 1).

Results

Families with hypokalaemic periodic paralysis mutations

HypoPP4 family with heterozygous $Na_V1.4$ R1135H (c.C3404A) mutation

The 47-year-old male proband had spontaneous paralytic attacks of up to 3-h duration, typically associated with slight hypokalaemia of 3.3 mM K^+. Onset was at age 16, and frequency was bi-monthly. Weakness was triggered by heavy meals, alcohol and stress. Oral K^+ salts ameliorated, and acetazolamide at 250 mg/d prevented these episodes. Oral glucose provocation with 2 g/kg together with 20 units of subcutaneous administration of insulin resulted in decreased serum K^+ from 4.1 to 3.4 mM (normal range 3.5 to 5.0 mM) and generalized muscle weakness lasting for several hours. In early adulthood, a fluctuating weakness of the upper limbs developed. Frequency and severity of paralytic attacks decreased after age 40 when moving to the warmer climate of Polynesia. A muscle biopsy revealed vacuolar myopathy containing tubular aggregates and focal, type 2 fibre atrophy. An excised specimen of muscle fibres was used for membrane potential measurements. Molecular genetics identified a heterozygous $Na_V1.4$ R1135H mutation. The mutation was found in his similarly affected mother, whereas it was excluded in each of two non-affected children.

HypoPP317 family with heterozygous $Na_V1.4$ R1135H (c.C3404A) mutation

At age 16 the 21-year-old proband with unaffected parents had cortisol-induced paraesthesias and muscle stiffness, and weakness in the extremities followed by weakness of trunk and respiratory muscles. In the intensive care unit, serum K^+ was markedly reduced to 1.9 mM and creatine kinase was slightly increased to 386 U/l (normal < 270). Infusion of 100 mEq potassium in 2.5 l solution administered over a 24-h period completely resolved the weakness.

In addition to endogenous spikes in cortisol levels (circadian peak in early morning, and after stress) and iatrogenic cortisol spike, other triggers were salt and liquorice, whereas cold temperature and exercise were not. In the 2 years after onset, episodes were bi-weekly and lasted 3 to 4 h. Two episodes were clinically similar to the Guillain-Barré syndrome and required hospitalization and intravenous K^+ administration because of

hypokalaemia of 2.3 and 3.0 mM, respectively. Since the last hospitalization, the patient has been taking 50 mg/d eplerenone in addition to daily potassium supplementation of 240 mEq. Molecular genetics identified a heterozygous $Na_V1.4$ R1135H mutation that seemed to be *de novo* as it was excluded in his non-affected parents.

^{1}H-MRI and ^{23}Na-MRI imaging have been used to detect muscular degeneration, oedema and sodium overload in hypokalaemic periodic paralysis patients harbouring R1 or R2 mutations of sodium or calcium channels (Jurkat-Rott *et al*., 2009). In the present study, ^{1}H-MRI of the R1135H patient at age 21 showed neither fatty degeneration nor muscular oedema. The ^{23}Na-MRI revealed a muscular sodium signal intensity of 0.97 when normalized to a 0.3% saline reference solution. This ratio was in the range of controls ($n = 10$; mean value ± SD: 0.99 ± 0.12, 95% confidence interval of 0.93–1.05) suggesting a weak effect of the mutation (Weber *et al*., 2006).

HypoPP181 family with homozygous $Na_V1.4$ R1135C (c.C3403T) mutation

The female proband had consanguineous healthy parents (first cousins). Her siblings had no muscle symptoms, and her daughter was not affected. The patient had the first episode at age 14, comprising a paralysis of neck and limb muscles, and respiratory difficulty with sudden onset and lasting 1 h. Initially the weakness episodes had a frequency of about three times per week, without having a clear precipitating factor. At a later stage in life, administration of catapresan for hypertension worsened her muscle symptoms, and convertan elicited attacks of respiratory weakness. Serum K^+ was checked several times with values mostly in the normal range, but at least for two episodes levels of 2.9 and 3.4 mM were noted, the latter despite a preceding oral K^+ ingestion. In the EMG there was no myotonia, and motor and sensory nerve conduction velocities were normal.

With time, episodic weakness became more frequent and some permanent weakness became evident. In the last years of her life she was wheelchair-bound most of the time. The permanent weakness motivated a biopsy of the biceps brachii muscle at age 60, revealing myopathy without biochemical alteration. Molecular genetics identified a homozygous $Na_V1.4$ R1135C mutation that was heterozygous in her non-affected daughter. Parents were unavailable for testing.

Intracellular action potentials

Action potentials in fibres harbouring the R1135H mutation revealed undershoots of −10.8 ± 9.5 mV instead of overshoots as in control fibres (+10.5 ± 7.9 mV, $P < 0.05$; Fig. 1A). The maximum rates of rise of R1135H action potentials were ~50% less than those from control fibres (Fig. 1B). The normalized maximum rates of rise, i.e. the steady-state slow inactivation curves, showed similar voltage dependence for R1135H and control fibres. Boltzmann fits to these curves yielded parameters of V_h $slow_{0.5} = -71.0$ mV and slope factor k = 8.0 mV (wild-type), compared with values of −74.8 mV and 9.3 mV for R1135H.

Resting membrane potentials

In 4 mM extracellular K^+, control and R1135H patient fibres showed a bimodal distribution of the resting potential. Gaussian fitting revealed peak values of P1 = −81.1 ± 0.3 and P2 = −58.7 ± 0.4 mV, similar to control fibres of P1 = −80.9 ± 0.1 and P2 = −60.2 ± 0.4 mV (Fig. 1C). However, more fibres were depolarized to P2 in the patient fibres as shown by the respective densities for P1 and P2, which were 0.38 ± 0.03 and 0.63 ± 0.05 compared with control fibres with values of 0.80 ± 0.03 and 0.04 ± 0.01 (Fig. 1C).

Decreasing the extracellular K^+ to 1 mM led to a tri-modal distribution for both patient and control fibres. Under these conditions, the peak values were tendentially shifted to more depolarized potentials for the patient fibres, i.e. peak values of the three populations for patient fibres were P1 = −86.4 ± 0.8, P2 = −66.7 ± 0.5 and P3 = −51.1 ± 0.8, compared with the control fibres with values of P1 = −89.7 ± 0.6, P2 = −72.7 ± 0.2 and P3 = −52.2 ± 0.5 (Fig. 1D). The density of the three peaks were 0.03 ± 0.02, 0.61 ± 0.05 and 0.29 ± 0.05 for patients, and 0.14 ± 0.03, 0.68 ± 0.03 and 0.25 ± 0.04 for controls, respectively. This can be interpreted as a borderline pathological result compatible with the diagnosis of hypokalaemic periodic paralysis. The ability of patients' fibres to repolarize after strong depolarizations in chloride-free solution was not markedly impaired with P1 = −85.7 ± 0.4 mV versus −79.9 ± 0.4 mV, P2 = −65.1 ± 1 mV versus −63.7 ± 1.1 mV for control and patients, respectively (Supplementary Fig. 1). This is in contrast to the single peak at −50 mV that fibres of hypokalaemic periodic paralysis patients show (Rüdel *et al*., 1984). Taken together, these results suggest a rather weak effect of the mutation.

Whole cell currents

Figure 2A displays typical recordings of depolarization-induced sodium currents elicited in tsA201 cells. The corresponding voltage-conductance curves according to a Boltzmann function are shown in Fig. 2B. Hypokalaemic periodic paralysis mutants displayed reduced voltage sensitivity with k = −11.38 ± 0.28 (R1135H) and −9.12 ± 0.21 (R1135C) versus −7.54 ± 0.16 (wild-type) as expected for neutralization of a positive charge in the S4 voltage sensor. Additionally, activation of R1135C was significantly left-shifted by almost 4 mV. In contrast, R1135H did not affect $V_{0.5}$, but slowed activation kinetics by a factor of ~1.5 (Fig. 2C). Activation is also slowed with histidine mutations in S4 of domain II (Kuzmenkin *et al*., 2002), perhaps as a result of the bulky side group added by that substitution.

Figure 2B shows steady-state inactivation curves for wild-type and mutant channels. Fits to a Boltzmann function revealed a significant left shift for both mutants, $V_{0.5} = -97.9 \pm 1.36$ mV (R1135H) and −100.8 ± 1.46 mV (R1135C) versus −84.7 ± 1.07 mV (wild-type), as well as a reduced slope k = 7.32 ± 0.19 (R1135H) and 8.83 ± 0.43 (R1135C) versus 5.80 ± 0.18 (wild-type). Additionally, the extent of closed state inactivation was markedly increased for both mutants (Fig. 2D). Both of these phenomena are consistent with the observed slow recovery from the fast inactivated state (Fig. 2E) fit by a

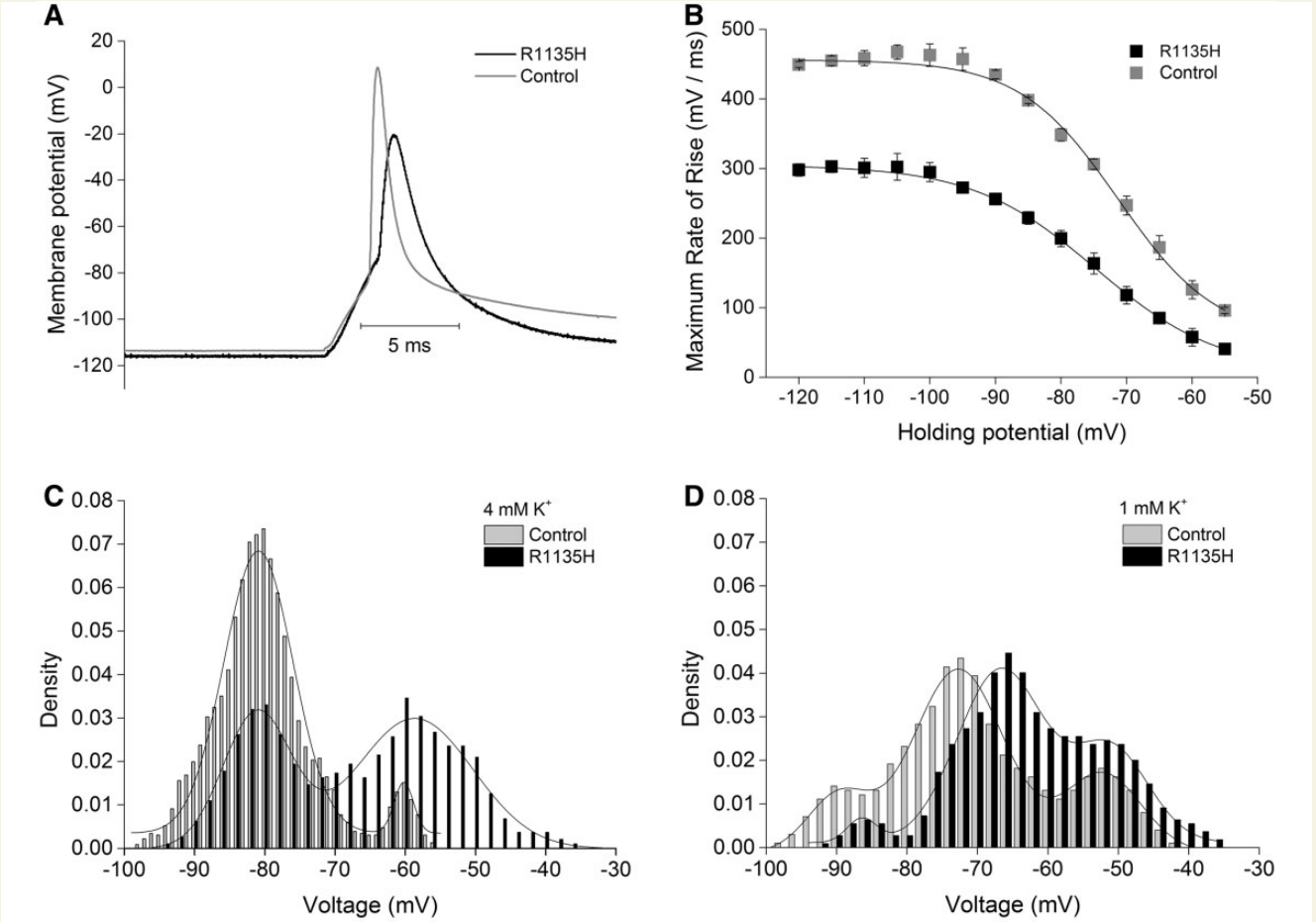

Figure 1 (**A**) Representative action potentials elicited from R1135H patient or wild-type control muscle fibres from 1 min holding potential of −120 mV. (**B**) Maximum rate of rise for R1135H patient ($n = 6$) and wild-type control ($n = 6$) fibres from varied holding potentials. (**C**) Bimodal distribution of membrane potentials of R1135H patient fibres ($n = 106$) and wild-type control fibres ($n = 256$) with 4 mM K^+ in the recording solution. Note the increased fraction of depolarized fibres in the patient. (**D**) Tri-modal distribution of membrane potentials of R1135H patient fibres ($n = 55$) and wild-type control fibres ($n = 61$) with decreased K^+ to 1 mM. Note the borderline depolarizing shift of the peak potentials in the patient fibres compared with controls.

two-exponential function, whereby the faster component differed significantly: $\tau_{FAST} = 7.47 \pm 0.72$ ms (R1135H) and 9.57 ± 1.26 ms (R1135C) versus 2.48 ± 0.22 ms (wild-type). Fig. 2F gives an overview of the time constants associated with fast inactivation for wild-type and mutant channels.

Results from experiments testing the effects of mutations on slow inactivation are shown in Supplementary Fig. 2. In wild-type channels, the midpoint of the steady-state slow inactivation curve $V_{SI\ 0.5}$ was -68.5 ± 1.38 mV, with a slope factor of 12.3 ± 0.7 mV (Supplementary Fig. 2A). R1135H produced a 4 mV left shift of $V_{SI\ 0.5}$ (-72.2 ± 1.3 mV, slope factor of 13.9 ± 0.98 mV), and R1135C produced a 6 mV left shift of $V_{SI\ 0.5}$ (-74.6 ± 1.46 mV, slope factor of 15.4 ± 1.11 mV). Wild-type channels entered into slow inactivation with a time constant of 4.37 ± 0.29 s, with 87% completion, compared with R1135H (4.44 ± 0.39 s, 91% completion) and R1135C (3.56 ± 0.31 s, 92% completion; Supplementary Fig. 2B). Recovery from slow inactivation was prolonged in hypokalaemic periodic paralysis mutants (Supplementary Fig. 2C), with time constants of 3.60 ± 0.52 s (R1135H) or 3.18 ± 0.35 s (R1135C), compared with 1.36 ± 0.08 s in wild-type channels.

Cut-open oocyte recordings

First, we measured leak currents in wild-type and mutant channels in experiments that compared the effect of external or internal substitution of small cations, guanidinium, or the large cation NMDG on outwardly or inwardly directed currents over the voltage range of −160 mV to +40 mV, from a holding potential of −100 mV. With Na^+, K^+ or Li^+ ion in the external solution, we did not observe an inwardly directed omega current similar to that for hypokalaemic periodic paralysis mutations at R1 or R2 in domains I to III of $Na_V1.4$ (data not shown). To test for an outwardly directed current in mutant channels, we performed experiments with cationic internal substitution (Fig. 3). rR1128H/C promoted a cation-selective, outwardly directed gating pore current with internal substitution of 60 mM guanidinium, and smaller outward currents with 115 mM Na^+, K^+ or Li^+ ion. These currents were

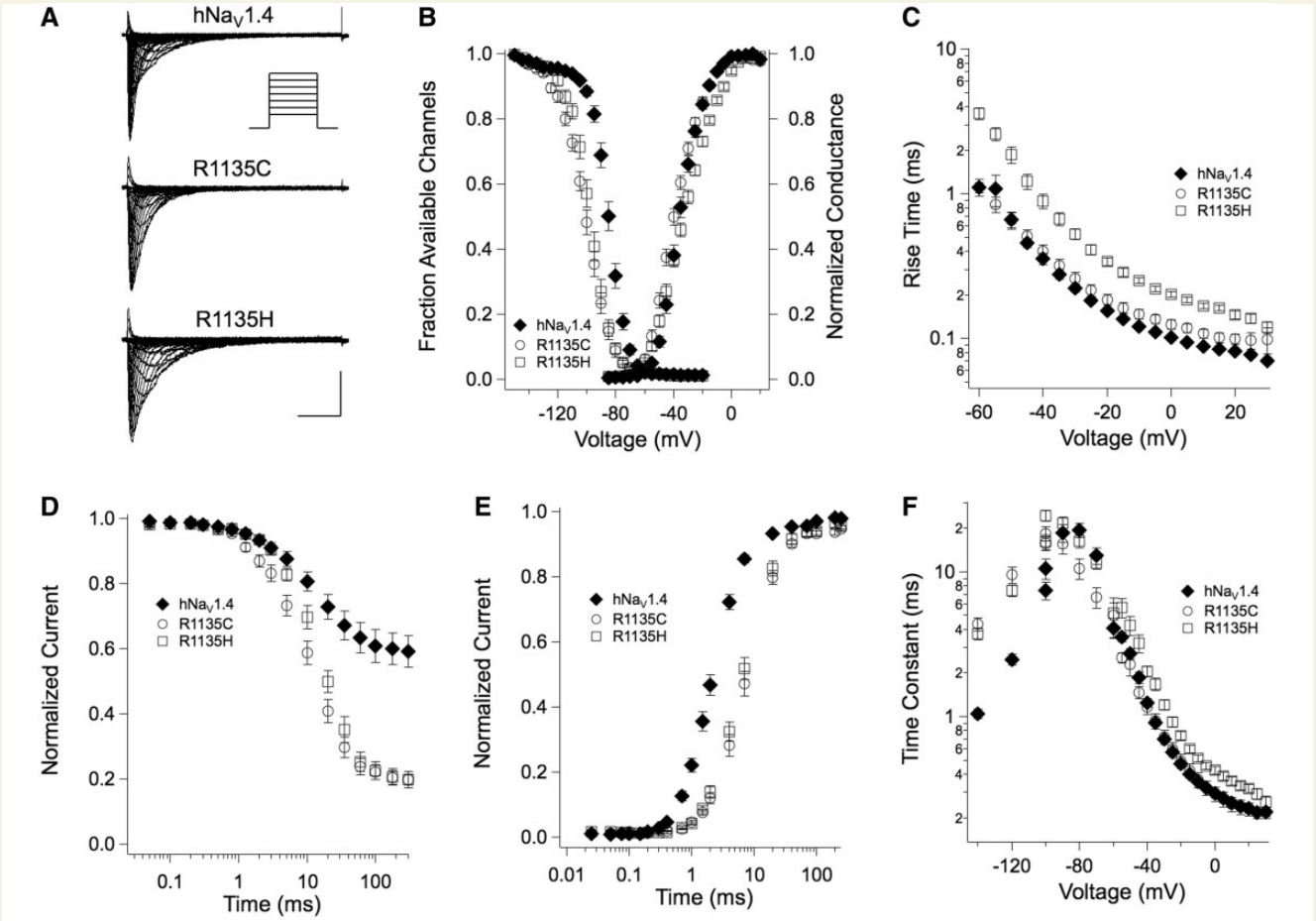

Figure 2 (**A**) Sodium currents elicited by depolarization to voltages ranging from −85 to +55 mV from a holding potential of −140 mV as recorded from tsA-201 cells expressing wild-type hNa$_V$1.4, R1135H, or R1135C channels. Calibration: horizontally, 5 ms; vertically, wild-type hNa$_V$1.4, R1135C 2 nA, R1135H 1.5 nA. (**B**) Conductance-voltage relationships from Boltzmann fits of steady-state activation and inactivation (n = 9–12). Steady-state fast inactivation was tested by a series of 300 ms depolarizing prepulses from −160 to −30 mV followed by a test pulse to −10 mV. (**C**) Kinetics of activation determined by the 10–90% rise time of sodium currents between −60 and +30 mV. (**D**) Time course of closed state inactivation for durations from 0.05 to 300 ms at −90 mV from a holding potential of −140 mV whereby a test pulse to −10 mV determined the fraction of non-inactivated channels. (**E**) Recovery from fast inactivation from a holding potential of −120 mV after an inactivating prepulse at −10 mV for 100 ms. (**F**) Voltage dependence of time constants of fast inactivation: for −140 to −100 mV, recovery from fast inactivation; for −100 to −70 mV, closed-state inactivation; for > −70 mV, open-state inactivation.

larger for rR1128C than for rR1128H and showed rectification at voltages more positive than −60 mV. With internal substitution of NMDG, or with oocytes injected with wild-type rNa$_V$1.4, leak currents exhibited a linear voltage dependence.

These experiments suggested that R3 is located below the gating pore in the resting state of the channel. We wished to test whether R3 is above the gating pore in the activated/inactivated states of the channel, to investigate the potential role of an omega current during recovery from fast inactivation for hypokalaemic periodic paralysis mutations. To move R3:DIIIS4 from below to above the gating pore constriction, we preconditioned oocytes to a holding potential of +40 mV for 100 ms before testing for leak currents over a voltage range of −160 mV to +40 mV (Fig. 4). With external substitution of 115 mM Na^+ or 60 mM guanidinium, channels with rR1128H/C mutations produced apparently inwardly rectifying currents, with the cysteine mutation producing larger currents.

In Fig. 4B, it is difficult to observe outward omega current because gradients are reversed compared with Fig. 3. To clarify whether the conditioning prepulse additionally occluded the omega pore, we examined raw leak current amplitudes with external sodium or guanidinium versus NMDG at −20 mV to +40 mV for wild-type and mutant channels without normalization. In wild-type rNa$_V$1.4 channels, leak currents at depolarized voltages were increased by 1.35-fold (sodium) and 1.52-fold (guanidinium), compared with currents elicited in NMDG. Relative leak current increases in sodium or guanidinium of 1.85- and 3.49-fold (rR1128H) and 2.57- and 3.05-fold (rR1128C), respectively, suggest that there is some population of mutant channels following preconditioning that have an open omega gating pore. At more

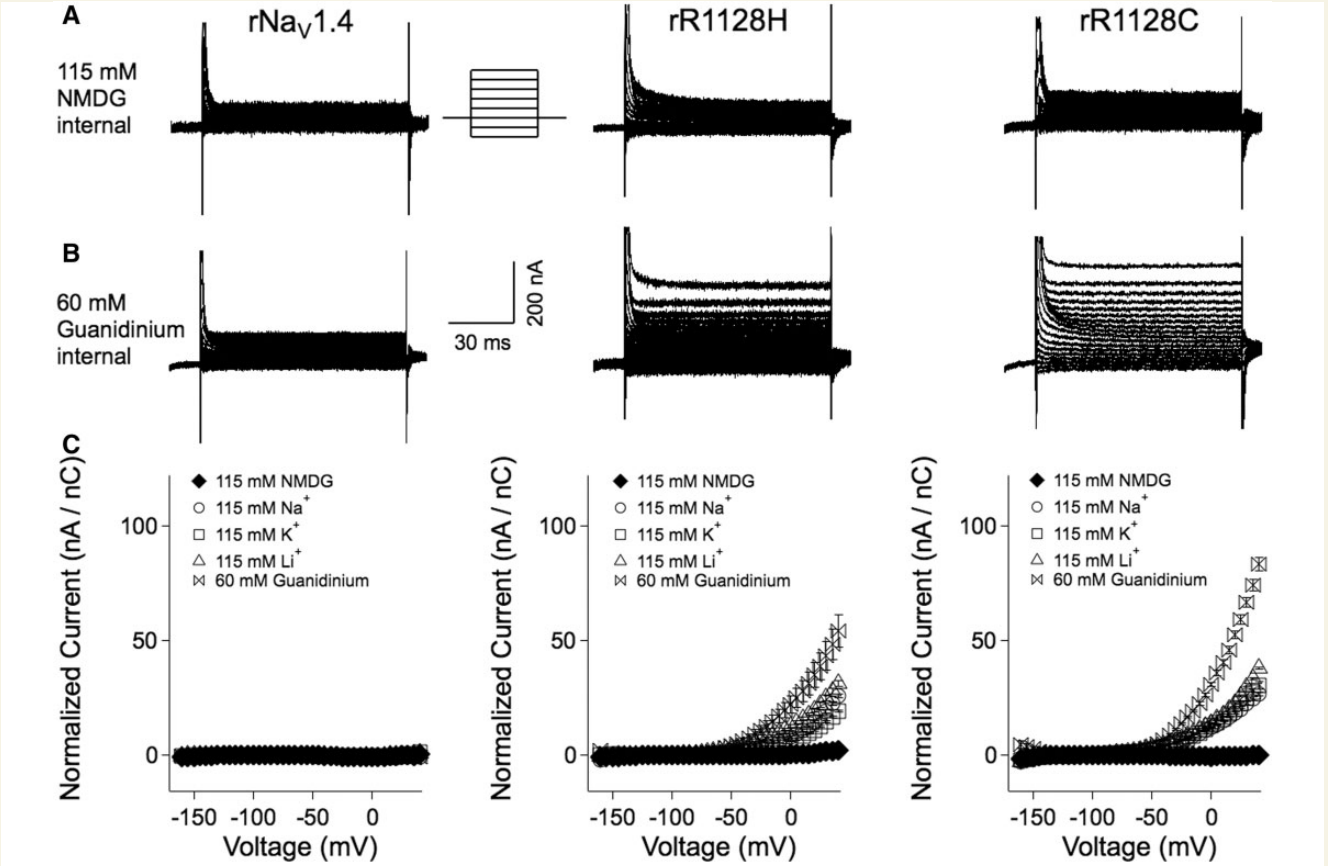

Figure 3 (**A**) Cut-open oocyte recordings of wild-type rNa$_V$1.4 and hypokalaemic periodic paralysis mutant channels with internal substitution of 115 nM NMDG. Traces are every other sweep showing non-subtracted currents in response to command potentials from −160 mV to +40 mV, from a holding potential of −100 mV. (**B**) Responses to same protocol, after internal substitution with 60 mM guanidinium / 60 mM NMDG. (**C**) Plots of normalized leak currents for wild-type and mutant channels for internal substitution of NMDG, monovalent cations or guanidinium. Currents were normalized with respect to gating charge integral recorded in response to +40 mV depolarization.

hyperpolarized potentials, it is likely that additional R3:DIIIS4 mutant residues enter that pore to produce the larger inwardly directed currents. We interpret these findings in the sense that the S4 movement during channel recovery is increasingly disturbed. To further examine this, we studied gating charge movement in wild-type and mutant channels, and modeled the molecular dynamics of the S4 translocation.

On and off gating current recordings

We performed gating current measurements of wild-type rNa$_V$1.4 and R3C/H using a protocol similar to that used in experiments shown in Fig. 4, to directly measure S4 deactivation with hyperpolarization from the inactivated state. We did this to investigate that possibility that hypokalaemic periodic paralysis mutations at R3:DIIIS4 slow the deactivation following fast inactivation, to explain the effect of these mutations to prolong recovery of channels.

The integral of the gating currents (charge) (Fig. 5A) was compared as Ig_{OFF} / Ig_{ON} for hyperpolarizing commands of durations up to 10 ms. Figure 5B shows the time course of deactivation, with command to −105 mV. An initial rapid rise in Ig_{OFF} / Ig_{ON} was observed for wild-type and mutant channels, reflecting the ~40% of gating charge that is unaffected (non-immobilized) by fast inactivation (Cha *et al*., 1999). The slower phase of deactivation was significantly prolonged in R3C/H, compared with wild-type channels.

The extent of the inhibition of S4 translocation in mutant channels compared with wild-type rNa$_V$1.4 is shown in Fig. 5C, with measurements taken as mean Ig_{OFF} / Ig_{ON} from 9.2 to 10 ms over the voltage range of −155 to −55 mV. Significantly less charge was returned in the mutant channels compared to wild-type for hyperpolarizing commands more negative than −70 mV; this effect produced by R3C/H is also observed in the current traces at 10 ms pulse duration shown in Fig. 5A. Importantly, our results show that hypokalaemic R3:DIIIS4 mutations disrupt the inward S4 translocation expected during recovery of channels from the fast inactivated state.

Molecular dynamics simulations

We used molecular dynamics simulations as an additional approach to investigate translocation of the voltage sensor of domain III in wild-type rNa$_V$1.4 and hypokalaemic periodic

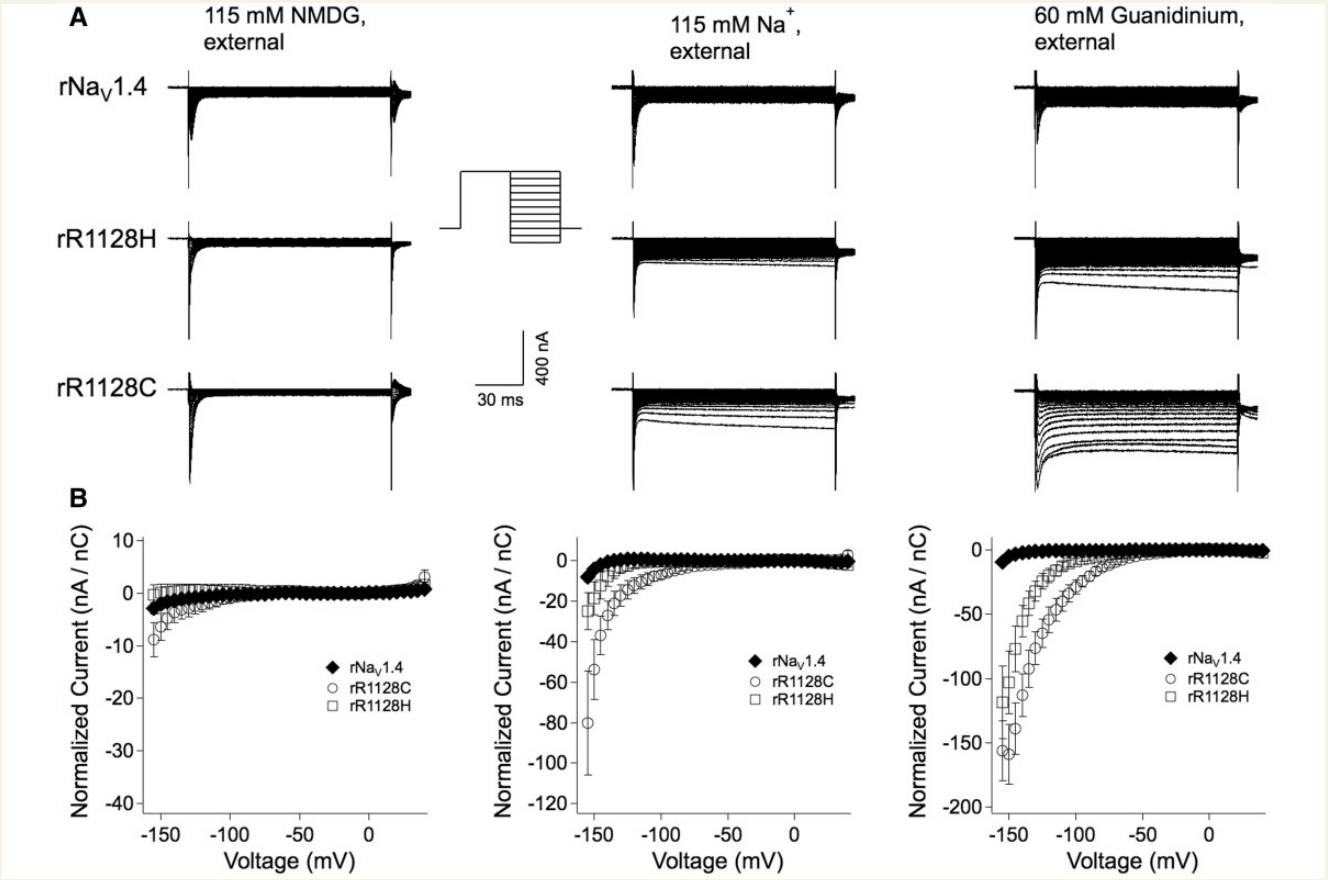

Figure 4 (**A**) Cut-open oocyte recordings of wild-type rNa$_V$1.4 and hypokalaemic periodic paralysis mutant channels during recovery from fast inactivation. From a holding potential of −100 mV, the oocyte membrane was held at +40 mV for 100 ms, before command test pulses at voltages from −160 mV to +40 mV. Traces shown (every other sweep) are responses in experiments with external solution of 115 mM NMDG, 115 mM Na^+, or 60 mM guanidinium. (**B**) Plots of normalized current amplitudes for each of the conditions shown in **A**.

paralysis channels, with conditions similar to those for electrophysiological experiments shown in Fig. 4. We did this to investigate whether the electrostatic interactions of DIIIS4 positive charges with negative countercharges suggested by recent studies (Gosselin-Badaroudine *et al*., 2012; Groome and Winston, 2013) are disrupted by the hypokalaemic periodic paralysis mutants at R3:DIIIS4 in a manner consistent with the findings from our functional studies. Figure 6A shows locations of relevant residues in the homology model of S1–S4 for domain III of rNa$_V$1.4. After equilibrating the protein in a POPC membrane *in silico* (Fig. 6B), negative potential was applied and the simulations were run for 10 ns (Fig. 6C). At the time points shown, proximities of side chains for DIIIS2 countercharges D1066 and E1076 with R2, R3/H3/C3, and R4 were measured, and are given in Supplementary Table 1.

For wild-type rNa$_V$1.4, R2 and R3 residues in S4 were each in close proximity (<3 Å) to upper negative countercharge D1066 in S2 at the start of simulation, as was R4 with the lower negative countercharge E1076 (Fig. 6C, top). At 4 ns into simulation, R2 and R3 were 6 Å or more distant from the upper S2 countercharge. Subsequently, the side chain of R3 passed the aromatic ring of F1073 to reside near E1076 in S2. At 10 ns, R4 was no longer in proximity to E1076.

MD simulations for rR1128H/C shown in Fig. 6C (middle and bottom panels) revealed several differences in countercharge to DIIIS4 interactions, compared to wild-type channels. For example, R3C and R3H were each 6 Å or more distant from D1066 at the start of simulation, and neither came in close proximity to E1076 in response to membrane hyperpolarization. For each R3 mutant channel, R2:D1066 and R4:E1076 proximities were similar to those for wild-type rNa$_V$1.4, at the start of simulation. However, in rR1128C the R2:D1066 proximity measurement remained within 3 Å throughout simulation, and for both mutants, R4 remained in close proximity to E1076.

Discussion

Genotype–phenotype correlation

Our results with native R1135H muscle fibres show that mutation at R3 increases the probability of depolarized resting membrane potentials under normal conditions. At low external potassium and after strong depolarizations in chloride-free solutions, the depolarization tendency is only marginal. Likewise, ^{23}Na-MRI showed a normal result. Additionally, the amplitude of the inward omega currents were only ~5% to 10% to those of R1 or R2 previously described (Sokolov *et al*., 2010). Furthermore, since inward omega currents only occur when IIIS4 has moved outward and been

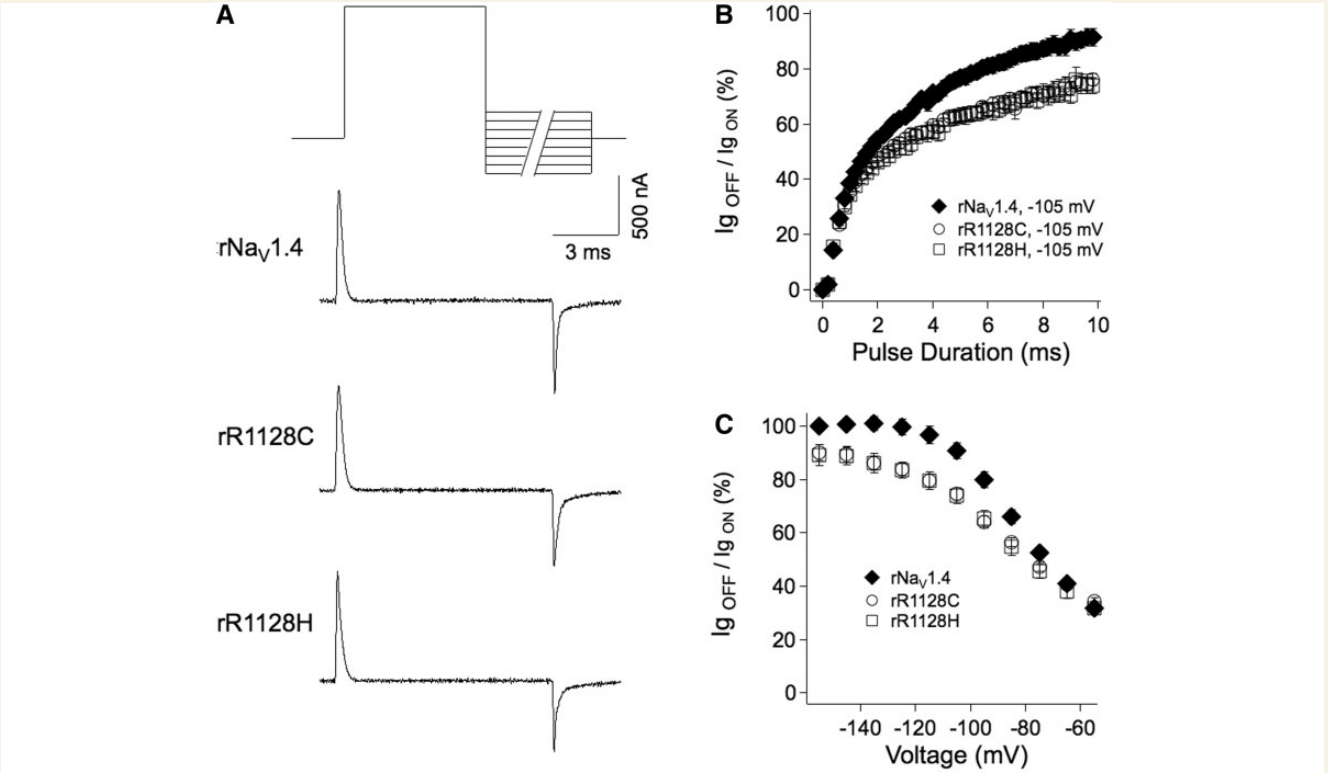

Figure 5 (**A**) Protocol used to measure on and off gating currents. Tetrodotoxin-blocked wild-type and mutant channels were depolarized for 30 ms to +40 mV to elicit Ig_{ON}, followed by a series of hyperpolarizing commands with variable voltage (−55 mV to −155 mV) and variable duration (0 to 10 ms in 0.2 ms intervals) to elicit Ig_{OFF}. Traces shown are for 10 ms command to −105 mV. (**B**) Kinetics of deactivation at −105 mV for pulse durations from 0 to 10 ms, expressed as the ratio of Ig_{OFF} / Ig_{ON}. (**C**) Voltage dependence of the effect of R3C/H to inhibit deactivation, measured at 9.2 to 10 ms hyperpolarizing pulse durations.

immobilized, they are not produced by the total mutant channel population but only by a portion of these, further reducing the effect of the mutation. Therefore, the effects of both mutations may indeed be slight.

As to the recessiveness of R1135C, we hypothesize that epigenetic factors or the differential effects of the two mutations on activation and recovery of the central pore current may be decisive for development of symptoms and the resulting mode of inheritance. As the dominant mutation R1135H slows all transitions presumably because of the bulkiness of the histidine residue, it could have a larger effect on the action potential and excitability in general than the recessive mutation R1135C.

Mechanisms for the effects of R3:DIIIS4 mutations

Effect of the outward omega currents

Recordings from patient muscle fibres showed an overall inexcitability, reduced amplitude and slowed rate of rise of action potentials. The reduced rate of rise to 50% action potential amplitude cannot be explained by depolarization-induced sodium channel inactivation, since we repolarized these fibres down to −120 mV for at least 1 min prior to action potential measurements. Cut-open oocyte recordings of R3:DIIIS4 mutations showed an outward omega current that is activated over the depolarized voltage range, a finding that is in agreement with earlier studies showing that mutations at R3:DIIS4 that cause normokalemic periodic paralysis (Vicart *et al*., 2004) also produce an outwardly directed omega current (Sokolov *et al*., 2008). Our action potential recordings therefore suggest that outward omega current in R3C/H may contribute to reduced excitability by shunting excitatory current through the gating pore in the depolarized voltage range for which action potential initiation is expected. In addition to its effect on action potential initiation, the outward omega current in R3C/H may provide a counteraction to chloride loss, explaining the ability of these fibres to repolarize in chloride-free solutions. This current may augment the intrinsic repolarizing mechanisms of ATPase and NKCC transporters (Lehmann-Horn and Jurkat-Rott, 1999). Possibly, the outward omega current is also able to reduce ictal hypokalaemia down to the mild levels found in these patients.

Effect of inward omega currents and disrupted S4 translocation

We found that each of the hypokalaemeic periodic paralysis mutations at R3:DIIIS4 impedes the downwards movement of S4, or deactivation, when channels were inactivated, and thus S4 is immobilized. The resulting small inward omega current is the basis for typical pathogenesis of hypokalaemic periodic paralysis as previously described (Cannon, 2010; Catterall, 2010; Tricarico

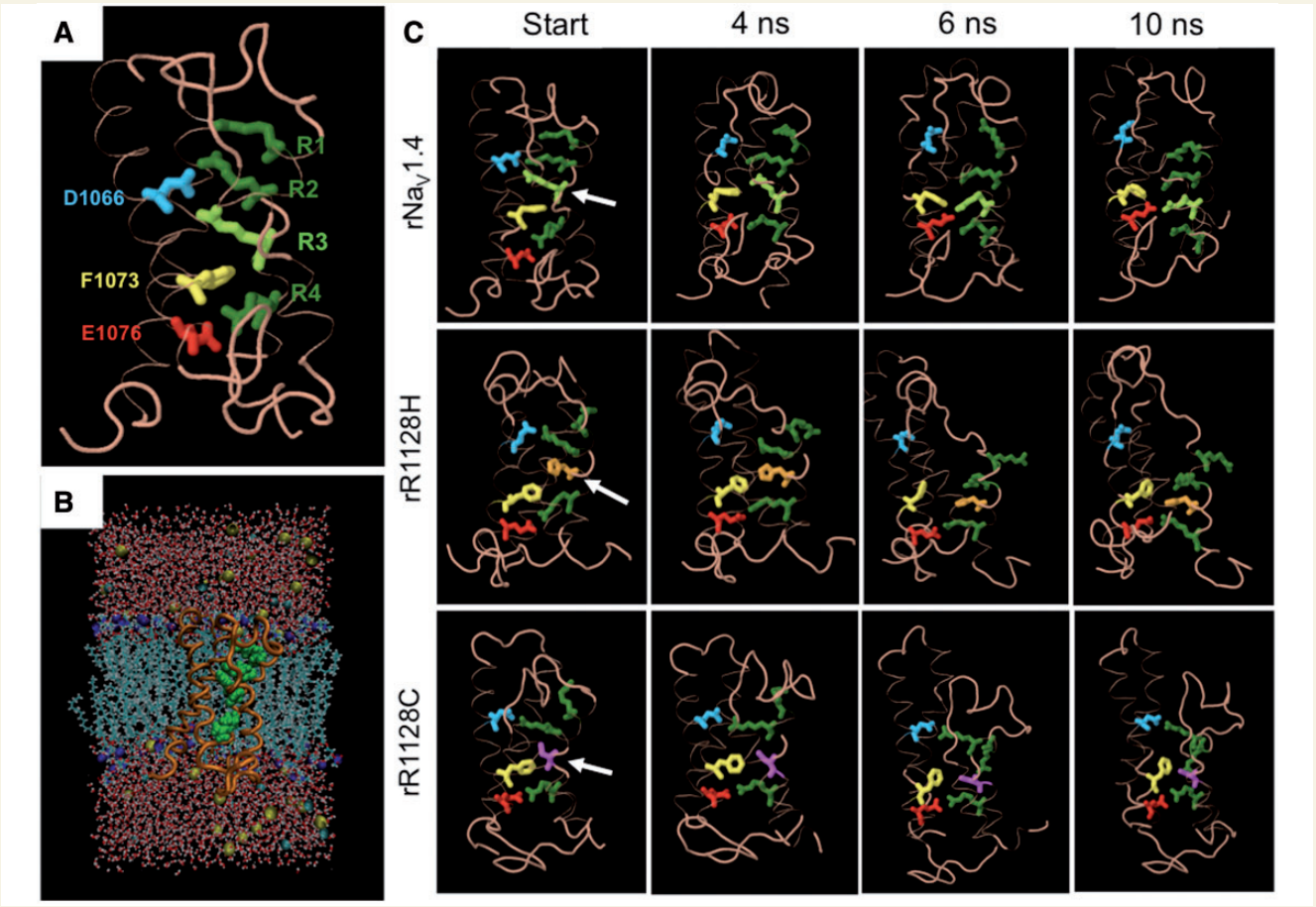

Figure 6 (**A**) Homology model of wild-type rNa$_V$1.4 DIII (domain III) voltage sensor module highlighting S2 and S4 residues; the R3 locus is in light green. (**B**) VSM model incorporated into POPC membrane. (**C**) Select frames at times shown for simulation of response to membrane hyperpolarization. Residue R3 (white arrow) is highlighted as light green (wild-type rNa$_V$1.4, *top*), orange (rR1128H, *middle*) or magenta (rR1128C, *bottom*). At each time, distance measurements were made for R2:D1066, R3/H3/C3:D1066, R3/H3/C3:E1076, and R4:E1076.

and Camerino, 2011; George, 2012; Jurkat-Rott *et al*., 2012). However, for the mutations at R3 the omega current is produced by a different mechanism than the previously described mutations, namely by a disturbed S4 movement during recovery from the inactivated state. Specifically, whereas S4 translocation and R3 passage upwards through the gating pore is relatively favourable, the reverse translocation is impeded and results in a prolonged non-occlusion of the pore i.e. enhancing the inward omega current. The effect of the hypokalaemic periodic paralysis mutations on S4 translocation may be their predominant effect to decrease membrane excitability in channels that have fast inactivated in the process of firing action potentials. For example, it has been shown that the voltage sensors in domains III and IV are immobilized during fast inactivation (Cha *et al*., 1999), with immobilization of the DIIIS4 sensor coupled to binding of the IFMT particle to its receptor (Sheets *et al*., 2000). Therefore, our finding that hypokalaemic periodic paralysis mutations at R3:DIIIS4 inhibit S4 translocation from a state of immobilization is consistent with the finding that these mutations slow the overall recovery of channels from fast inactivation.

Molecular dynamics simulations support the results of gating current measurements that show R3C/H impedes S4 translocation during deactivation. Proximity measurements taken during these trajectories suggest that DIIIS2 countercharges may be an important substrate of voltage sensor translocation during recovery, and that the effect of hypokalaemic periodic paralysis mutations involves a decreased interaction of those S2 countercharges with R3 as the S4 segment traverses the gating pore towards the resting state. This hypothesis is supported by a previous study using molecular dynamics to investigate intermediate states of voltage sensor translocation in rNa$_V$1.4 (Gosselin-Badaroudine *et al*., 2012). In that simulation of wild-type rNa$_V$1.4, interaction of R3:DIIIS4 with the outer S2 charge (D1066) is proposed for the activated state of the channel, whereas interaction of R3:DIIIS4 with an inner S2 charge (E1076) is proposed for intermediate and resting states. Additionally, R4 interacts with E1076 in the activated and intermediate, but not resting state. Each of these interactions was reiterated in our simulations of rNa$_V$1.4. By incorporating the hypokalaemic periodic paralysis mutations into our simulations, we found that R3H/C each may have limited

interaction with the outer and inner S2 residues during voltage sensor translocation, and that the R4:E1076 interaction persists in the resting state of the channel. Therefore, we propose that R3:DIIIS4 hypokalaemic periodic paralysis mutations disrupt native electrostatic interactions in the voltage sensor module necessary for recovery.

Acknowledgements

We thank Dr M. A. Weber, DKFZ Heidelberg, for performing the MRI.

Funding

This work was supported by NIH 1R15NS064556-01 to J.R.G. and NIH P20 RR016454 to I.S.U., by the non-profit Else-Kröner-Fresenius foundation and the German BMBF Ministry for the IonNeurOnet project and the DGM jointly to K.J.R. and F.L.H. F.L.H. is endowed Senior Research Professor of Neurosciences of the non-profit Hertie-Foundation. K.J.R. is a fellow of the Hertie-Foundation. The work was also supported by the Eva Luise Köhler Stiftung.

Supplementary material

Supplementary material is available at *Brain* online.

References

Cannon SC. Voltage sensor mutations in channelopathies of skeletal muscle. J Physiol 2010; 588: 1887–95.

Catterall WA. Ion channel voltage sensors: structure, function, and pathophysiology. Neuron 2010; 67: 915–28.

Cavel-Greant D, Lehmann-Horn F, Jurkat-Rott K. The impact of permanent muscle weakness on quality of life in periodic paralysis: a survey of 66 patients. Acta Myologicia 2012; 31: 126–33.

Cha A, Ruben PC, George AL Jr, Fujimoto E, Bezanilla F. Voltage sensors in domains III and IV, but not in I and II, are immobilized by Na^+ channel fast inactivation. Neuron 1999; 22: 73–87.

Cohen CJ, Bean BP, Tsien RW. Maximal upstroke velocity as an index of available sodium conductance. Comparison of maximal upstroke velocity and voltage clamp measurements of sodium current in rabbit Purkinje fibers. Circ Res 1984; 54: 636–51.

Delemotte L, Tarek M, Klein M, Amaral C, Treptow W. Intermediate states of the $K_V1.2$ voltage sensor from atomistic molecular dynamics simulations. Proc Natl Acad Sci USA 2011; 108: 6109–14.

Fontaine B. Periodic paralysis. Adv Genet 2008; 63: 3–23.

Francis DG, Rybalchenko V, Struyk A, Cannon SC. Leaky sodium channels from voltage sensor mutations in periodic paralysis, but not myotonia. Neurology 2011; 76: 1–7.

George AL Jr. Leaky channels make weak muscles. J Clin Invest 2012; 122: 4326–33.

Gosselin-Badaroudine P, Delemotte L, Moreau A, Klein ML, Chahine M. Gating pore currents and the resting state of $Na_V1.4$ voltage sensor domains. Proc Natl Acad Sci USA 2012; 109: 19250–5.

Groome JR, Winston V. S1-S3 counter charges in the voltage sensor module of a mammalian sodium channel regulate fast inactivation. J Gen Physiol 2013; 141: 601–18.

Jurkat-Rott K, Lehmann-Horn R, Elbaz A, Heine R, Gregg RG, Hogan K, et al. A calcium channel mutation causing hypokalemic periodic paralysis. Hum Mol Genet 1994; 3: 1415–19.

Jurkat-Rott K, Mitrovic N, Hang C, Kouzmekine A, Iaizzo P, Herzog J, et al. Voltage sensor mutations cause hypokalemic periodic paralysis type 2 by enhanced inactivation and reduced current. Proc Natl Acad Sci USA 2000; 97: 9549–54.

Jurkat-Rott K, Weber M-A, Fauler M, Guo X-H, Holzherr BD, Paczulla A, et al. K^+-dependent paradoxical membrane depolarization and Na^+ overload, major and reversible contributors to weakness by ion channel leaks. Proc Natl Acad Sci USA 2009; 106: 4036–41.

Jurkat-Rott K, Groome JR, Lehmann-Horn F. Pathophysiological role of omega pore current in channelopathies. Front Neuropharmacol 2012; 3: 1–15.

Khalili-Araghi F, Tajkhorshid E, Roux B, Schulten K. Molecular dynamics investigation of the ω-current in the $K_V1.2$ voltage sensor domains. Biophys J 2012; 102: 258–67.

Kuzmenkin A, Muncan V, Jurkat-Rott K, Hang C, Lerche H, Lehmann-Horn F, et al. Enhanced inactivation and pH sensitivity of Na+ channel mutations causing hypokalemic periodic paralysis type II. Brain 2002; 125: 825–43.

Lehmann-Horn F, Jurkat-Rott K. Voltage-gated ion channels and hereditary disease. Physiol Rev 1999; 79: 1317–72.

Matthews E, Labrum R, Sweeney MG, Sud R, Haworth A, Chinnery PF, et al. Voltage sensor charge loss accounts for most cases of hypokalemic periodic paralysis. Neurology 2009; 72: 1544–7.

Payandeh J, Scheuer T, Zheng N, Catterall WA. The crystal structure of a voltage-gated sodium channel. Nature 2011; 475: 353–8.

Rüdel R, Lehmann-Horn F, Ricker K, Küther G. Hypokalemic periodic paralysis: *in vitro* investigation of muscle fiber membrane parameters. Muscle Nerve 1984; 7: 110–20.

Sheets MF, Kyle JW, Hanck DA. The role of the putative inactivation lid in sodium channel gating current immobilization. J Gen Physiol 2000; 115: 609–19.

Sokolov S, Scheuer T, Catterall WA. Ion permeation through a voltage-sensitive gating pore in brain sodium channels having voltage sensor mutations. Neuron 2005; 47: 183–9.

Sokolov S, Scheuer T, Catterall WA. Gating pore current in an inherited ion channelopathy. Nature 2007; 446: 76–8.

Sokolov S, Scheuer T, Catterall WA. Depolarization-activated gating pore current conducted by mutant sodium channels in potassium-sensitive normokalemic periodic paralysis. Proc Natl Acad Sci USA 2008; 105: 19980–5.

Sokolov S, Scheuer T, Catterall WA. Ion permeation and block of the gating pore in the voltage sensor of $Na_V1.4$ channels with hypokalemic periodic paralysis mutations. J Gen Physiol 2010; 136: 225–36.

Struyk AF, Cannon SC. A Na^+ channel mutation linked to hypokalemic periodic paralysis exposes a proton-selective gating pore. J Gen Physiol 2007; 130: 11–20.

Struyk AF, Markin VS, Francis D, Cannon SC. Gating pore currents in DIIS4 mutations of $Na_V1.4$ associated with periodic paralysis: saturation of ion flux and implications for disease pathogenesis. J Gen Physiol 2008; 132: 447–64.

Sung CC, Cheng CJ, Lo YF, Lin MS, Yang SS, Hsu YC, et al. Genotype and phenotype analysis of patients with sporadic periodic paralysis. Am J Med Sci 2012; 343: 281–5.

Tricarico D, Camerino DC. Recent advances in the pathogenesis and drug action in periodic paralyses and related channelopathies. Front Pharmacol 2011; 2: 1–8.

Weber M-A, Nielles-Vallespin S, Essig M, Jurkat-Rott K, Kauczor HU, Lehmann-Horn F. Muscle Na^+ channelopathies: MRI detects intracellular ^{23}Na accumulation during episodic weakness. Neurology 2006; 67: 1151–8.

Vicart S, Sterberg D, Fournier E, Ochsner F, Laforet P, Kuntzer T, et al. New mutations of *SCN4A* cause a potassium-sensitive normokalemic periodic paralysis. Neurology 2004; 63: 2120–7.